

DEVELOPMENT OF DRAG-REDUCED TURBULENT BOUNDARY LAYERS ON SMOOTH WALLS WITH DIFFERENT POLYMER CONCENTRATIONS

Mohamed G. AbdElKader, John R. Elsnab, Nicholas Hutchins, and Jason P. Monty

Department of Mechanical Engineering
University of Melbourne
Parkville Victoria 3010 Australia
mabdelkaderg@student.unimelb.edu.au

ABSTRACT

A range of polyacrylamide concentrations was used to investigate the development of drag-reduced turbulent boundary layers over a towed flat-plate. A unique experiment was built where a 5 m-long plate was towed through a large volume of uniform concentration polymer solution. Time-resolved particle image velocimetry data of instantaneous streamwise wall-normal velocity fields were obtained owing to the unique frame of reference of the tow tank facility. Results reveal that the presence of polymer significantly affects the outer region coherent structure of the turbulent boundary layer, via damping of small-scale vortices and the formation of high-strength long shear layers.

INTRODUCTION

The turbulent flow of polymer solutions at minute concentrations displays a significant skin friction drag reduction of nearly 80% relative to the turbulent flow of the solvent (usually water) alone (White & Mungal, 2008). This phenomenon is of great importance as it potentially leads to substantial energy savings in marine and liquid transportation applications. Since the discovery of the effect of polymers on the turbulent boundary layer by Toms (1948), extensive research has been aimed to describe the limitations and cause of the phenomenon. A variety of experimental, (Virk *et al.*, 1967; Warholic *et al.*, 1999; White *et al.*, 2004; Winkel *et al.*, 2009; Elsnab *et al.*, 2019) and numerical (Sureshkumar *et al.*, 1997; De Angelis *et al.*, 2002; Dubief *et al.*, 2004) investigations in internal and external flow systems, reveal the main characteristics which describe the turbulent boundary layer modifications due to polymer presence.

The reduction of skin friction drag is accompanied by modifications to the turbulent boundary layer statistics. One such modification is the slope change of the mean streamwise velocity profile. Virk (1975) reported an upward shift in the inner-scaled mean velocity profile logarithmic region at lower drag reduction rates (Newtonian plug) and a slope increase in this region with further drag reduction rise until an asymptotic drag reduction value is attained. Additionally, the mean inner-scaled streamwise turbulence intensity increases with polymer concentration with its inner-scaled peak moving further away from the wall, which was found to have a linear trend with the percentage of drag reduction in the low drag-reduction regime (Elsnab *et al.*, 2019).

The effect of polymer on the turbulent boundary layer coherent structure has been investigated using experimental flow visualization and simulation techniques. Warholic *et al.* (2001) used particle image velocimetry (PIV) to obtain in-

stantaneous velocity fields of polymer drag-reduced turbulent channel flow. He noticed damping in small-scale vortices in the near-wall region accompanied by a reduction in the inner-scaled wall-normal turbulent intensity. These modifications reveal a measurable interaction between polymers and turbulence, especially the interaction with near-wall vortices and velocity streaks, which represents the turbulence regeneration cycle (Jiménez & Pinelli, 1999). Further research by White *et al.* (2004) using wall-parallel-plane PIV detected a coarsening and organization of the low-speed velocity streaks at 50% drag reduction. Dubief *et al.* (2004) used numerical simulation to describe the role of polymer stretching and relaxing in disturbing the near-wall vortices and energizing the streamwise velocity fluctuation. However, the detailed polymer-turbulence interaction is still a subject of study, especially for the high drag reduction regime (White & Mungal, 2008).

Despite the intensive research on the drag-reduced turbulent boundary layer characteristics, only a few studies investigated external flow applications (e.g., ship hulls, submarine surface). Most of the external flow experiments dealt with the behaviour of the turbulent boundary layer after polymer injection, with a consequent variation of polymer concentration across the boundary layer, e.g., Fontaine *et al.* (1992); Winkel *et al.* (2009). The current research investigates the effect of uniform polyacrylamide concentration (polymer ocean) on the development of turbulent boundary layers over a flat-plate. This study gives clearer insight into drag-reduced turbulent boundary layer structure and the effect of different uniform polymer concentrations, namely 25, 50, and 100 ppm, on such flow structure in the outer region.

EXPERIMENTAL SETUP

Experiments were conducted in the Michell Hydrodynamics Laboratory at the University of Melbourne using the tow tank facility (see figure 1). The facility consists of a 60 m × 2 m × 2 m (L × W × H) tank equipped with overhead rails on both tank sides. A carriage travels back and forth with minimal vibration along 30 m of the tank length at a speed up to 1.5 m/s. A horizontally mounted flat-plate of plan area, 5 m × 1.2 m (L × W), is suspended from the carriage inside the tank. The tank side is equipped with a 1.0 m × 1.5 m viewing glass window for under water optical access located at 21.6 m from the plate start position. The total length of the tank was divided into three sections separated by two barriers 1.0 m × 1.8 m to isolate the water between the barriers (middle section) from the rest of the tank water. The total distance travelled by the plate is contained within the middle tank section

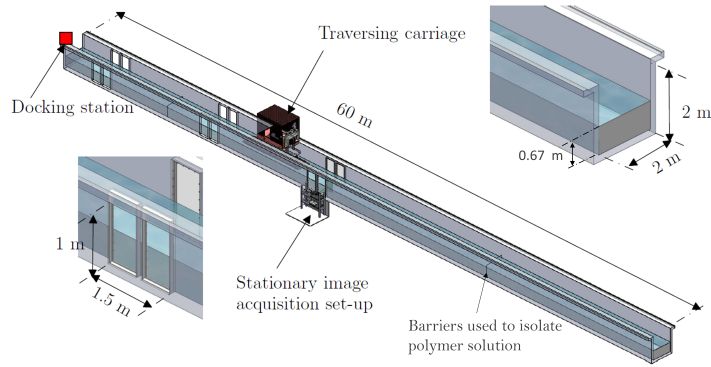


Figure 1. Schematic of tow tank facility at the University of Melbourne

30 m \times 2 m. Such a setup was chosen to reduce the amount of polymer required to obtain the desired concentration in such a large facility. All the experiments presented here were conducted in the middle tank section of the facility, referred to as the 'test-section', while the plate traversed between the barriers. The volume of the water in the test-section is approximately 41000 L. The flow at the upstream end of the plate was tripped using ≈ 1 mm diameter wire, which slightly overstimulates the turbulent boundary layer based on the study by Erm & Joubert (1991).

The polymer used in the current experiment is water-soluble anionic polyacrylamide (APAM) manufactured by Gongyi Xinqi Chemical plant (anionic polyacrylamide 9260), and has an average molecular weight, M_w (g/mol), of 6 million according to manufacturer specifications. The preparation process of the polymer solution was challenging due to the large volume of the test-section. For example, a 100 ppm concentration requires 4.1 kg of APAM. The preparation process of the aqueous polymer solution was carefully made in several steps. Firstly, the necessary amount of polymer was measured using a precision scale (Sartorius Entris224-1s) with a maximum weight capacity of 220 g and resolution of 0.1 mg. Secondly, the weighed powder was divided into batches to produce a highly concentrated polymer solution in a 100 L external tank using water from the test-section. The concentrated solutions were stirred using a spiral mixer at 30 rpm to reduce the polymer mechanical degradation during the solution preparation process. Thirdly, the final polymer solution was made by introducing these batches to the test-section across the water surface area. Finally, the solution was left in the tank for two days to ensure complete homogeneous polymer mixing across the test-section. The final polymer concentration was checked using an Ubbelohde viscometer. The viscometer is manufactured and calibrated by CANNON Instrument Company. The concentration check process starts by carefully preparing small samples with concentrations equivalent to the required test-section concentrations (25, 50, 100 ppm) and then comparing the viscosity of such samples with the ones collected from the test-section at different locations and times. The test-section samples were collected before, during and after each experiment to ensure a constant polymer concentration throughout the experiment. The collected and reference samples were kept at a constant temperature of 16°C during viscosity measurement. The change of solution viscosity with polymer concentration for the reference samples is presented in figure 2(a). The linear fit to the data was used to estimate the polymer concentration based on the solution

viscosity for the collected samples. The data presented in figure 2(a) indicates that the change in concentration is less than 13% for all the experiments conducted in the current study. Furthermore, the variation of solution kinematic viscosity with time is presented in figure 2(b). The figure displays that a constant viscosity is maintained throughout each experiment. Six samples were collected every measurement day, and the error bars represent the 95% confidence interval for such samples. For data analysis, the solution viscosity for all cases was taken as that for the solvent due to the small concentrations used in the current study.

Time-resolved x - z instantaneous velocity fields were acquired where x , y and z are the streamwise, spanwise, and wall-normal coordinates, respectively, and u , v and w indicate the corresponding velocity components. Each data set was obtained by towing the plate through the field of view at a constant speed $U_\infty \approx 0.9$ m/s ($Re_x = 9.5 \times 10^5 - 4.5 \times 10^6$ for the Newtonian case). The PIV setup used in the current study consists of two PCO dimax HS4 CMOS cameras with 32GB buffer. The field of view illumination is supplied by a Photonics DM20-527 dual head Nd:YLF laser that delivers 100 mJ/pulse at 1000 Hz. Each time the plate is towed past the stationary PIV system, we acquire ≈ 5000 instantaneous velocity fields capturing the streamwise development of the drag-reduced turbulent boundary layer. The acquired images are processed using an in-house PIV processing. The image processing algorithm uses a multigrid interrogation analysis with a final interrogation window size of 32×32 pixels, equivalent to 1.5 mm \times 1.5 mm in real space with 50% overlap. The number of passes acquired for the pure water (Newtonian) and polymer solution (non-Newtonian) cases is 100 and 85, respectively, which requires five days for the non-Newtonian experiments. The total number of passes used produces a statistical convergence for the mean streamwise velocity, U . However, we need at least 700 passes to reach turbulent intensity convergence as discussed by Lee (2017), which was not possible in the current study due to time limitations.

RESULTS

The parameters for the different experimental cases are summarised in table 1. The development of the momentum thickness, θ , is shown in figure 3(a) along the streamwise plate length, x_{plate} . From figure 3(a), it is shown that the momentum thickness at a given x location reduces as the polymer concentration increases, indicative of an increasing drag reduction. The friction velocity, u_τ , was calculated using the momentum integral equation for the zero pressure gradient tur-

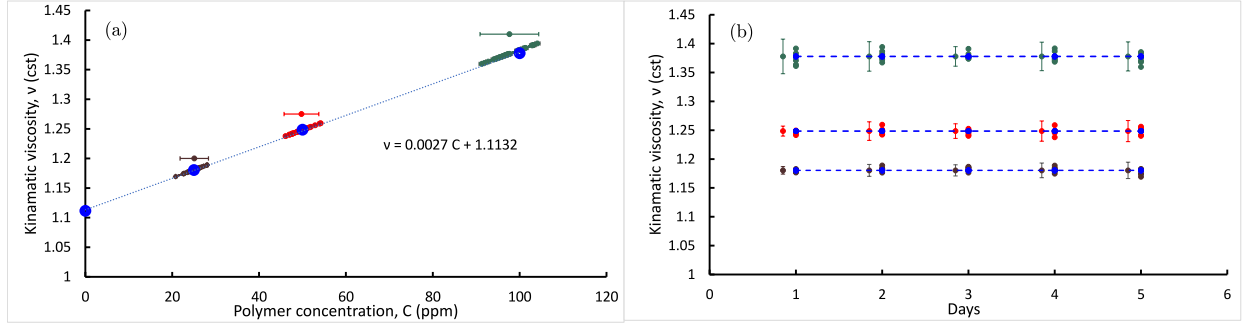


Figure 2. (a) Solution kinematic viscosity vs. polymer concentration as measured using the Ubbelohde viscometer at 16°C. • reference samples and the displayed equation represent the trendline equation fitting the reference samples. • 25 ppm, • 50 ppm, and • 100 ppm. The error bars represent the 95% confidence interval for each case (13% viscosity variation for 25 ppm). (b) Kinematic viscosity variation with time during the different concentration experiments. The error bars represent the 95% confidence interval per day.

bulent boundary layer

$$\frac{d\theta}{dx} = \frac{C_f}{2} = \left(\frac{u_\tau}{U_\infty} \right)^2, \quad (1)$$

where C_f is the coefficient of friction and U_∞ is the free stream velocity. The boundary layer thickness, δ_{99} , used for computing θ is identified as the location where the streamwise velocity reaches 99% of the free stream velocity. The streamwise gradient of the momentum thickness, $d\theta/dx$, was calculated by numerical differentiation using the presented θ vs x_{plate} profile. Since the output is noisy, as expected from numerical differentiation, a fitting equation was used to smooth the results based on the assumption that Re_θ has a log-linear relationship with the coefficient of friction C_f as presented by Österlund *et al.* (2000); Jiménez & Pinelli (1999). The following fit was assumed, $C_f = A \log(Re_\theta) + B$, where A and B are the fitting constants. The fitting to the developing C_f obtained for the Newtonian case is presented in figure 3(b). Note that the fitting points start at $x_{plate} \gtrsim 1$ m from the trip wire to avoid any interference from the trip wire on the obtained C_f .

The coefficient of friction, C_f , variation along the plate length as a function of the streamwise Reynolds number Re_x for the Newtonian case is plotted and compared with the computed predictions in figure 3(c). The solid lines represent the fittings by Schlichting, White and Nikuradse as modified by Nagib *et al.* (2007) for the canonical turbulent boundary layer. The calculated C_f is in good agreement with the predictions. The discrepancy at the lower Re_x is attributed to the proximity of the measurement location to the trip wire. Table 1 also includes the friction Weissenberg number, $We_\tau = \lambda u_\tau^2 / \nu$, which is the ratio of the polymer relaxation time, λ , to the viscous time scale and represents the viscoelastic effect of the solution. λ , was calculated using Zimm (1956) theory provided in

$$\lambda = 0.422 \frac{[\eta] M_w \mu_s}{N_A k_B T}, \quad (2)$$

where $[\eta] = 0.01 M_w^{0.755}$ is the intrinsic viscosity for APAM solution Kulicke *et al.* (1982), μ_s is the solvent (water) dynamic viscosity, N_A is Avogadro's number, k_B is the Boltzmann constant, and T is the solution temperature. The Zimm theory is valid for dilute polymer solutions below the overlap concentration, C^* , which can be

Table 1. Different experimental cases in the current study at $x_{plate} = 2.4$ m

Case	δ_{99} (mm)	Re_τ	%DR	We_τ	Symbols
Newtonian	42	1561	0	0	□
25 ppm	32	935	35.4	1.08	*
50 ppm	22	544	56.4	0.732	x
100 ppm	19.9	422	65.5	0.575	▽

determined using $C^* = 1/[\eta]$. In the present study, the critical overlap concentration C^* is 763 ppm, which indicates that all the current concentration is in the dilute regime.

The non-Newtonian friction velocity estimation was performed using the same procedure as the Newtonian one. Although the logarithmic fitting procedure has no physical basis for the non-Newtonian cases, we find a good fit to the measured C_f for $x_{plate} \gtrsim 1$ m. The percentage drag reduction is calculated using

$$\%Dr = \frac{\tau_N - \tau_{Non}}{\tau_N} \times 100, \quad (3)$$

where τ_N and τ_{Non} are the Newtonian wall and non-Newtonian wall shear stress, respectively.

Inner-scaled mean streamwise velocity U^+ profiles at $x_{plate} = 2.4$ m from the trip wire are presented in figure 4(a). The dashed line represents data from the turbulent boundary layer simulation provided by Eitel-Amor *et al.* (2014) at a comparable Reynolds number, and the solid line represents the maximum drag reduction asymptote as provided by Virk (1975). For the Newtonian case, a good collapse is observed beyond $z^+ \approx 100$ between the experimental streamwise mean velocity profile and the simulation reference data at comparable $Re_\tau = 1561$. For the non-Newtonian case, the errorbar represents $\pm 5\%$ error in the u_τ assumption as calculated using the error analysis criteria provided by Moffat (1988). Figure 4(b) presents the normalized mean streamwise u'^2 . The discrepancies found in the figure near the wall are a result of the lower PIV interrogation window spatial resolution and the lower

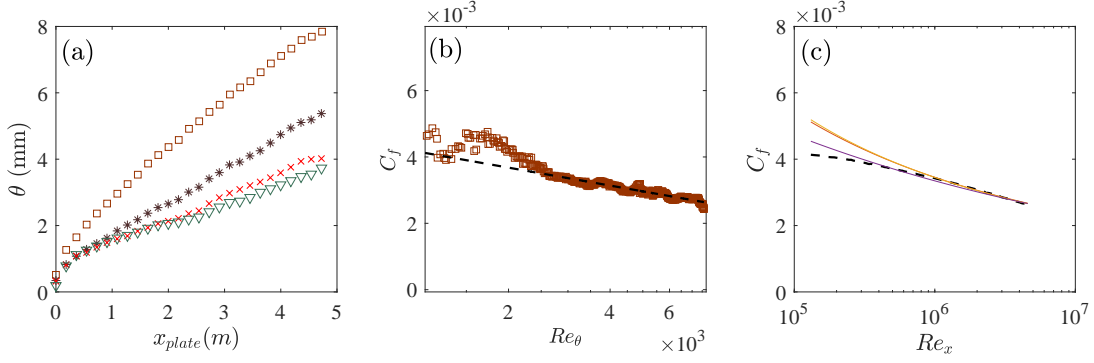


Figure 3. (a) Development of the momentum thickness θ along the plate length x_{plate} in meters ($Re_x = 9.5 \times 10^5 - 4.5 \times 10^6$) for different polymer concentrations add. Symbols description is presented in table 1, (b) Calculated coefficient of friction C_f based on the momentum integral equation for the Newtonian case, --- the log-linear fitting, $C_f = A \log(Re_\theta) + B$, with $A = -8 \times 10^{-4}$ and $B = 9.6 \times 10^{-3}$, (c) the comparison between the calculated C_f from fitting for the Newtonian case and --- Schlichting fit $(2 \log_{10}(Re_x) - 0.65)^{-7/3}$, — White $0.4177(\log(0.06Re_x))^{-2}$ and — Nikuradse $0.02666Re_x^{-0.1502}$.

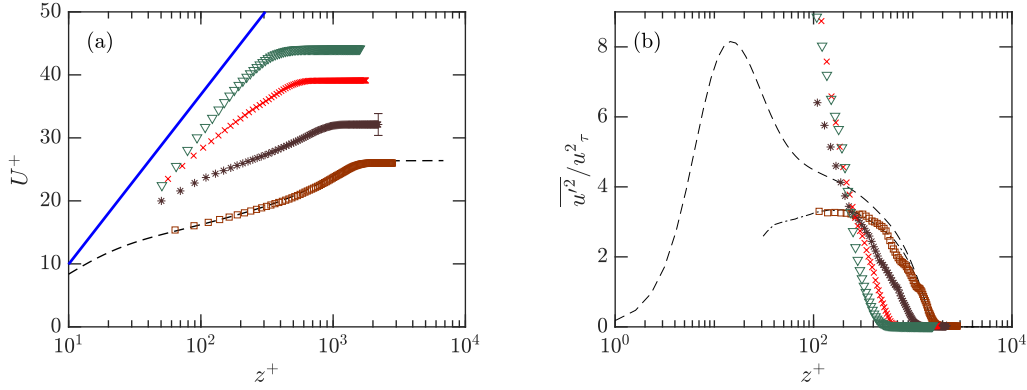


Figure 4. Mean statistics for the different experimental results at $x_{plate} = 2.4$ m. (a) Mean streamwise velocity, U^+ , (b) Mean streamwise turbulence intensity, $\overline{u'^2}$. The blue line represents the Virk's asymptote, $11.7 \log(z^+) - 17$. The black dashed lines represent the statistical reference data from Eitel-Amor *et al.* (2014). The dashed dot line is the under-resolved statistics using estimation tool from Lee *et al.* (2016). The error bar represents $\approx 5\%$ error due to the method used to calculate u_τ . Symbols definition is presented in table 1.

number of samples used to calculate the mean statistics (only 100 realizations were used for every plate position x_{plate}), which is not adequate for second order statistics convergence in the current experiment (Lee, 2017).

The black dashed line in figure 4(b) shows the DNS data of Eitel-Amor *et al.* (2014) at comparable Re_τ to the Newtonian case. Due to the effect of spatial resolution, the PIV resolved variance is below this curve. The black dot-dashed line shows the predicted DNS result at a matched resolution to the PIV experiment, using the predictive tool of Lee (2017). This serves as a further validation of these measurements, demonstrating that any discrepancy between the PIV and DNS for the Newtonian case is entirely attributable to spatial attenuation and the unconverged turbulence intensities. Additionally, figures 4(a,b) illustrate the typical effect of the drag-reducing polymer on the turbulent boundary layer. Such effect appears in the upward shift in the logarithmic layer of the inner-scaled mean velocity profile for low drag reduction cases and the increasing of the inner-scaled near-wall streamwise turbulence intensity with increasing polymer concentration.

A snapshot of the acquired real space instantaneous spanwise vorticity fields in the streamwise wall-normal plan is shown in figures 5(a,b) for Newtonian and 100 ppm non-Newtonian cases, respectively. The colorbar represents the magnitude of the spanwise vorticity squared ω_y^2 . The boundary layer thickness of the drag-reduced turbulent boundary layer at 100 ppm ($\delta_{99} \approx 20$ mm) is approximately half of the Newtonian one ($\delta_{99} = 42$ mm) as observed from figures 5(a,b). To better compare the details of the coherent structures, the outer-scaled field of view for the same vorticity field is presented in figures 5(c,d). The vorticity field of the non-Newtonian case indicates a reduction in the number of small-scale vortices, and the formation of high-strength, more coherent and elongated inclined vortical fissures or shear layers in the outer layer. Zadrazil *et al.* (2012) also observed the presence of shear layers in the vorticity field of pipe drag reduced turbulent flow using polymer injection. However, The features in the current study extend to $z \approx \delta$ in the outer region of the drag reduced turbulent boundary layer. These modifications become more observable with drag reduction increase. On

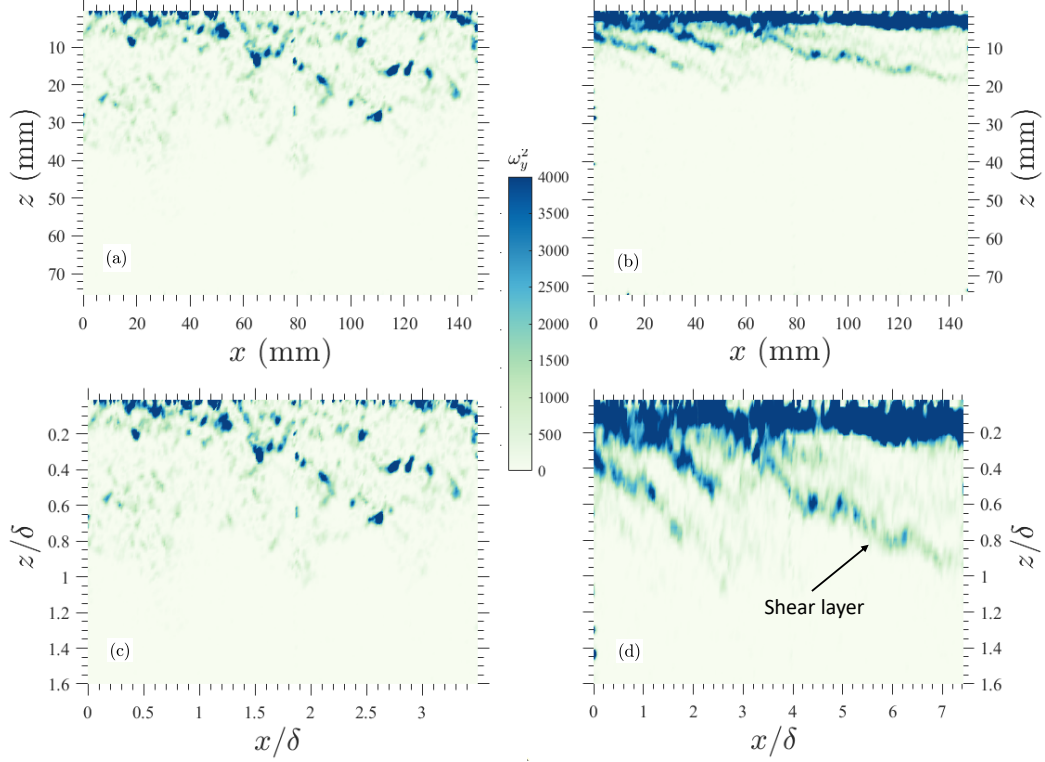


Figure 5. Moving plate frame of reference x - z plane of the spanwise vorticity strength ω_y^2 at $x_{plate}=2.4$ m ($Re_x \approx 2.25 \times 10^6$). (a) and (c) pure water (Newtonian) %DR = 0 and (b) and (d) 100 ppm polymer concentration (non-Newtonian) %DR = 65 of the developing turbulent boundary layer on smooth wall. The plate is moving from right to left. (a) and (b) dimensional coordinates, (c) and (d) outer-normalized coordinates.

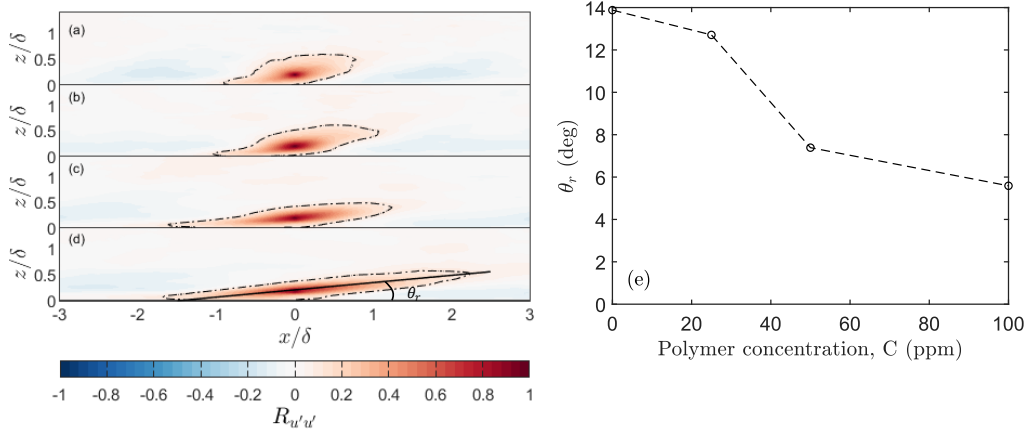


Figure 6. Mean 2-pt correlation for the streamwise velocity fluctuation R_{uu} for $x_{plate}=2.4$ m and $z_{ref} = 0.2\delta$. (a) Newtonian, (b) 25 ppm, (c) 50 ppm, and (d) 100ppm. The dashed dot line shows the larger principal axis as determined from the principal component analysis. (e) the change in the correlation feature inclination angle, θ_r , with polymer concentration.

the other hand, The Newtonian turbulent boundary layer shows scattered features in the vorticity field. The drag-reduced turbulent boundary layer coherent structure can also be assessed from the normalized two-point correlation for the streamwise velocity fluctuation field $R_{u'u'}$ as shown in figure 6 for $x_{plate} = 2.4$ m, and reference position $z_{ref} = 0.2\delta$. The normlized cross correlation coefficient was calculated using

$$R_{uu} = \frac{u'(x, z)u'(x + \Delta x, z + \Delta z)}{\sigma_{u'_x} \sigma_{u'_{x+\Delta x, z+\Delta z}}}, \quad (4)$$

where σ is the standard deviation of the corresponding signal. It shows that the mean coherent structure is gradually squeezed in the wall-normal direction and elongated in the streamwise direction with increasing polymer concentration. The black dashed lines in figures 6(a–d) represent the contour for $R_{u'u'}=0.1$. The contour extends to $\approx 4\delta$ for $R_{u'u'}=0.1$ in the streamwise direction for the 100 ppm case, which is the highest polymer concentration investigated in the current study. Furthermore, the coherent inclination angle was determined using the principal component analysis

(PCA). The angle of the major axes obtained from PCA is used as the feature inclination angle, θ_r , an example of which is given by the solid line on figure 6(d). Modification to this computed angle with polymer concentration is shown in Figure 6(e). As presented, the angle becomes smaller while increasing polymer concentration. Fontaine *et al.* (1992) also calculated the principal stresses using the scatter plot of the streamwise and wall-normal velocity fluctuations and found a decrease in the major principal stress axis angle with drag reduction.

CONCLUSION

It is well known that polymers significantly affect the near-wall region of the turbulent boundary layer. In this study, an investigation for the boundary layer region $z > 0.2\delta$ is presented using a uniform polyacrylamide concentration (polymer ocean). A homogenous concentration eliminates the effect of polymer mixing accompanied by the injection process on the turbulence features. The polymer has a noticeable effect on the outer region vortical structure. Such effect is observed in the presence of high-strength and elongated features that extend to $z \approx \delta$. Two-point correlations of streamwise velocity fluctuations show an extended feature in the order of 4δ in the streamwise direction at high drag reduction, approximately 2–3 times the length of the structure in the Newtonian case. The inclination angles of these features were determined using the principal component analysis. Such angles decrease with increasing polymer concentration. These findings indicate that the polymer effect extends to the outer region of the turbulent boundary layer.

REFERENCES

- De Angelis, E., Casciola, C. M. & Piva, R. 2002 DNS of wall turbulence: Dilute polymers and self-sustaining mechanisms. *Comput. Fluids* **31** (4), 495–507.
- Dubief, Y., White, C. M., Terrapon, V. E., Shaqfeh, E. S. G., Moin, P. & Lele, S. K. 2004 On the coherent drag-reducing and turbulence-enhancing behaviour of polymers in wall flows. *J. Fluid Mech.* **514**, 271–280.
- Eitel-Amor, G., Örlü, R. & Schlatter, P. 2014 Simulation and validation of a spatially evolving turbulent boundary layer up to $Re = 8300$. *Int J Heat Fluid Fl* **47**, 57–69.
- Elsnab, J. R., Monty, J. P., White, C. M., Koochesfahani, M. M. & Klewicki, J. C. 2019 High-fidelity measurements in channel flow with polymer wall injection. *J. Fluid Mech.* **859**, 851–886.
- Erm, L. P. & Joubert, P. N. 1991 Low-Reynolds-number turbulent boundary layers. *J. Fluid Mech.* **230**, 1–44.
- Fontaine, A. A., Petrie, H. L. & Brungart, T. A. 1992 Velocity profile statistics in a turbulent boundary layer with slot-injected polymer. *J. Fluid Mech.* **238**, 435–466.
- Jiménez, J. & Pinelli, A. 1999 The autonomous cycle of near-wall turbulence. *JFM* **389**, 335–359.
- Kulicke, W. M., Kniewske, R. & Klein, J. 1982 Preparation, characterization, solution properties and rheological behaviour of polyacrylamide. *Prog. Polym. Sci.* **8** (4), 373–468.
- Lee, J. H., Kevin, Monty, J. P. & Hutchins, N. 2016 Validating under-resolved turbulence intensities for PIV experiments in canonical wall-bounded turbulence. *Exp. Fluids* **57** (8), 129.
- Lee, J. H. W. 2017 Evolution of canonical turbulent boundary layers. PhD thesis, University of Melbourne.
- Moffat, R. J. 1988 Describing the uncertainties in experimental results. *Exp. Therm. Fluid Sci.* **1** (1), 3–17.
- Nagib, H. M., Chauhan, K. A. & Monkewitz, P. A. 2007 Approach to an asymptotic state for zero pressure gradient turbulent boundary layers. *Philos. T. R. Soc. A.* **365** (1852), 755–770.
- Österlund, J. M., Johansson, A. V., Nagib, H. M. & Hites, M. H. 2000 A note on the overlap region in turbulent boundary layers. *Phys Fluids* **12** (1), 1–4.
- Sureshkumar, R., Beris, A. N. & Handler, R. A. 1997 Direct numerical simulation of the turbulent channel flow of a polymer solution. *Phys Fluids* **9** (3), 743–755.
- Toms, B. A. 1948 Some observations on the flow of linear polymer solutions through straight tubes at large Reynolds numbers. *Proc. of In. Cong. On Rheology, 1948* **135**.
- Virk, P. S. 1975 Drag reduction fundamentals. *AIChE J.* **21** (4), 625–656.
- Virk, P. S., Merrill, E. W., Mickley, H. S., Smith, K. A. & Mollo-Christensen, E. L. 1967 The Toms phenomenon: Turbulent pipe flow of dilute polymer solutions. *J. Fluid Mech.* **30** (2), 305–328.
- Warholic, M. D., Heist, D. K., Katcher, M. & Hanratty, T. J. 2001 A study with particle-image velocimetry of the influence of drag-reducing polymers on the structure of turbulence. *Exp. Fluids* **31** (5), 474–483.
- Warholic, M. D., Massah, H. & Hanratty, T. J. 1999 Influence of drag-reducing polymers on turbulence: Effects of Reynolds number, concentration and mixing. *Exp. Fluids* **27** (5), 461–472.
- White, C. M. & Mungal, M. G. 2008 Mechanics and prediction of turbulent drag reduction with polymer additives. *Annu. Rev. Fluid Mech.* **40** (1), 235–256.
- White, C. M., Somandepalli, V. S. R. & Mungal, M. G. 2004 The turbulence structure of drag-reduced boundary layer flow. *Exp. Fluids* **36** (1), 62–69.
- Winkel, E. S., Oweis, G. F., Vanapalli, S. A., Dowing, D. R., Perlin, M., Solomon, M. J. & Ceccio, S. L. 2009 High-Reynolds-number turbulent boundary layer friction drag reduction from wall-injected polymer solutions. *J. Fluid Mech.* **621**, 259–288.
- Zadrazil, I., Bismarck, A., Hewitt, G. F. & Markides, C. N. 2012 Shear layers in the turbulent pipe flow of drag reducing polymer solutions. *Chem. Eng. Sci.* **72**, 142–154.
- Zimm, Bruno H. 1956 Dynamics of polymer molecules in dilute solution: Viscoelasticity, flow birefringence and dielectric loss. *J. Chem. Phys.* **24** (2), 269–278.